

# Transmission electron microscopy of the pyrometamorphic breakdown of phengite and chlorite

R. H. WORDEN, P. E. CHAMPNESS AND G. T. R. DROOP

*Department of Geology, University of Manchester, Oxford Road, Manchester, M13 9PL*

## Abstract

Phengite and chlorite have undergone decomposition during pyrometamorphism caused by the intrusion of a dolerite feeder pipe into Dalradian greenschists in Argyllshire, Scotland. All reaction products are extremely fine grained. Transmission electron microscopy has revealed that phengite pseudomorphs consist of biotite, spinel, mullite, sanidine and phengite, and that chlorite pseudomorphs consist of combinations of chlorite, spinel, orthopyroxene, magnetite, cordierite and biotite. Although the reactions were short-lived and did not go to completion, microprobe analysis and phase diagram analysis have revealed that there has been significant chemical interaction between the phyllosilicates and the surrounding rock. Numerous orientation relationships exist between the original minerals and their reaction products; the close-packed planes in the precursor phyllosilicates were inherited by their reaction products.

KEYWORDS: reaction mechanism, electron microscopy, pyrometamorphism, phengite, chlorite.

## Introduction

METAMORPHIC reactions and reaction mechanisms are one of the most important keys to the understanding of metamorphic petrogenesis. As most reactions go to completion, preservation of earlier disequilibrium assemblages rarely occurs. Where reaction textures are preserved, kinetic controls have been predominant, preventing the rock from achieving thermodynamic equilibrium. Such kinetic controls may be low diffusion rates, low fluid pressure or a limited period of time at peak metamorphic conditions.

Various metamorphic reactions in rocks with textures coarse enough to be investigated by light optics have been studied by Carmichael (1969), Foster (1977) and Chinner (1962). However, as the early stages of metamorphism involve reaction over very small distances, many important details of the reaction may go unobserved using light optics or conventional electron microprobe analytical techniques. The most suitable instrument for the study of fine grained crystalline features is the transmission electron microscope fitted with an X-ray spectrometer.

Few studies have been made on prograde metamorphic reactions using the transmission electron

microscope. The only previously published studies are those of Brearley (1984, 1986), who investigated the breakdown of phengite in a Moine xenolith from a dolerite dyke, and Wirth (1985), who studied the breakdown of phengite from glaucophane schists in the aureole of a quartz diorite intrusion.

In this study the TEM was used to examine the pyrometamorphic breakdown of phengite and chlorite in a contact aureole, situated near the summit of Sithean Sluagh, 2.8 km south-west of Strachur, Argyllshire, Scotland. The physical conditions of metamorphism and the mineral chemistries are significantly different from the samples studied by Brearley (1984, 1986) and Wirth (1985).

*Background geology.* The intrusion responsible for the pyrometamorphism discussed in this study is thought to be of Tertiary age and a feeder-pipe, rather than a static body (Smith, 1969). The country rocks are Dalradian greenschists of the 'Garnetiferous Misc Schist Group' of Hill *et al.* (1905). Before contact metamorphism, these schists were formed during garnet zone regional metamorphism at a temperature of approximately 450 °C and a pressure between 5 and 7 kbar during the Grampian orogeny.

The central part of the igneous intrusion is gabbroic with a surrounding dolerite ring-dyke

(Smith, 1969). This implies injection and solidus temperatures in excess of 1000 °C. On consideration of the age of the intrusion, rates of erosion and the thickness of the Tertiary basalt sheet, Smith (1969) estimated the pressure during pyrometamorphism to have been 0.5 kbar. The intrusion, which forms a kidney-shaped outcrop measuring 300 by 100 m, has produced an aureole of 12 m maximum visible extent. Exposure is very poor beyond this limit.

The Dalradian rocks are interbedded psammites, pelites and greenstones. Outside the aureole these rocks possess a well-developed schistosity which is locally crenulated. Major regional metamorphic minerals are quartz, albite, phengite and chlorite. The minor minerals, in approximately decreasing order of abundance, are garnet, biotite, calcite, epidote, ilmenite, pyrite, tourmaline and apatite.

### Light optical studies

Rocks which were only partially affected by the pyrometamorphism and which are therefore most likely to contain kinetically frozen reaction textures, were collected at 12 m from the contact at the north east edge of the intrusion. Smith (1969) says of these rocks: 'At this stage of metamorphism each grain has acted as a more or less isolated chemical system' and 'most micaceous material is somewhat altered. The larger areas of chlorite have turned greenish-brown . . . some muscovite has broken down but still retains appreciable birefringence'.

This implies that each grain may be treated as an isolated chemical system and the sum of the compositions of the reaction products should be the same as the parent phase. The likelihood that phyllosilicates, and especially the muscovite/phengite, have only partially reacted, and that all reaction products are very fine-grained, makes them fertile ground for transmission electron microscopy. The average grain size of the reaction products is well below the limits of resolution of light optics or the electron microprobe.

In these rocks other reaction textures are visible. The presence of a colourless glass of low refractive index at quartz-quartz grain boundaries provides evidence of incipient melting. This implies the presence of a grain boundary fluid, since, in the absence of water, pure silica begins to melt at about 1700 °C at 0.5 kbar. Albite has become cloudy in places and also shows signs of having started to melt along fractures.

Textures become progressively coarser towards the contact. Within 2 m of the contact, well annealed assemblages of corundum, cordierite, hercynite, mullite, magnetite and pseudobrookite have developed (Smith 1965, 1969), indicative of

very high temperatures. Inner- and middle-aureole rocks have approached thermodynamic equilibrium and are unlikely to contain stranded reaction textures.

### Electron microprobe analysis

Mineral analyses were carried out by standard microprobe techniques using a Cameca Camebax, operating at 15 kV. Analyses were obtained for minerals in country rocks and for chlorite and phengite pseudomorphs from the outer aureole. In anhydrous minerals, the ferric iron total is calculated assuming fixed stoichiometry. In hydrous minerals all iron is assumed to be ferrous iron.

*Analysis of country rocks.* Table 1 shows the range of phengite compositions. These have fairly high celadonite components, from 20 to 40 mole %, and paragonite components average 10 mole %. Celadonite substitution for muscovite obeys the Tschermak rule:



The phengite has a higher proportion of Si and lower Al relative to pure muscovite because of the Tschermak substitution. Also the phengite is iron-rich and Ti poor, the latter reflecting the low temperatures of peak regional metamorphism (Kwak, 1968; Guidotti, 1973).

Chlorite, with compositions shown in Table 2, falls within the ripidolite field as defined by Hey (1954). Within this field, the chlorite tends to be iron-rich. These compositions are typical of chlorites produced during low- to medium-grade regional metamorphism (Miyashiro, 1973).

Biotite analyses are plotted in Fig. 1, which shows the range of biotite compositions made possible by Fe-Mg and Tschermak substitutions. This diagram will be used to compare compositions of biotites produced during pyrometamorphism to those of regional metamorphic origin.

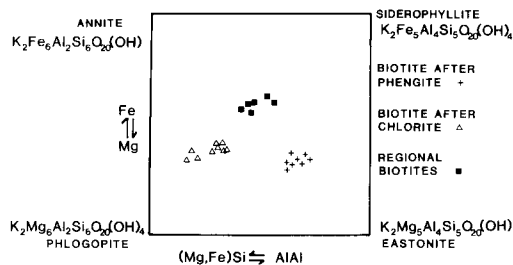


FIG. 1. Biotite end-member diagram showing the compositional range. Differences between the regional metamorphic biotites and the two pyrometamorphic biotites are illustrated.

*Analysis of phengite and chlorite pseudomorphs.* Analyses were carried out in order to determine the extent to which the chemistry of each grain had altered during the pyrometamorphism. The results of analyses across individual pseudomorphs are shown graphically in Figs. 2 and 3. In the case of phengite (Fig. 2)  $\text{SiO}_2$  and  $\text{Na}_2\text{O}$  increase, and  $\text{Al}_2\text{O}_3$ ,  $\text{K}_2\text{O}$ ,  $\text{FeO}$  and  $\text{MgO}$  decrease toward grain margins. The centres of these pseudomorphs represent phengite that has retained much of its original chemistry; the grain edges interacted with the surrounding rock and have undergone most chemical change. Analyses of chlorite pseudomorphs display a similar pattern of increasing interaction toward the pseudomorph margin (Fig. 3) with  $\text{SiO}_2$  and  $\text{K}_2\text{O}$  increasing and  $\text{FeO}$  and  $\text{MgO}$  decreasing towards the edge of the grain, while  $\text{Al}_2\text{O}_3$  remains constant throughout. Transfer of material has clearly taken place between the reacting phyllosilicate grains and surrounding grains. Therefore it is clearly invalid to assume that each grain has acted as an isolated chemical system.

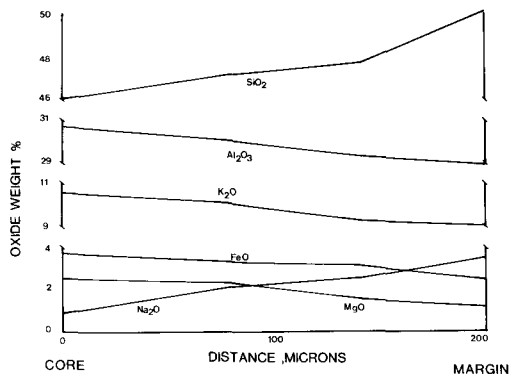


FIG. 2. Compositional variation diagram, illustrating the differences across a phengite pseudomorph adjacent to quartz.

### Electron microscopy

Specimens were prepared for the transmission electron microscope using the ion-beam thinning techniques described by Barber (1970) and Tighe (1976).

Electron microscopy was performed in a Philips EM400T, operating at 120 kV with either a tungsten or a  $\text{LaB}_6$  filament. Analyses were carried out using the EDAX energy-dispersive system and the thin-film approximation of Cliff and Lorimer (1975), whereby absorption and fluorescence corrections were applied for an estimated sample

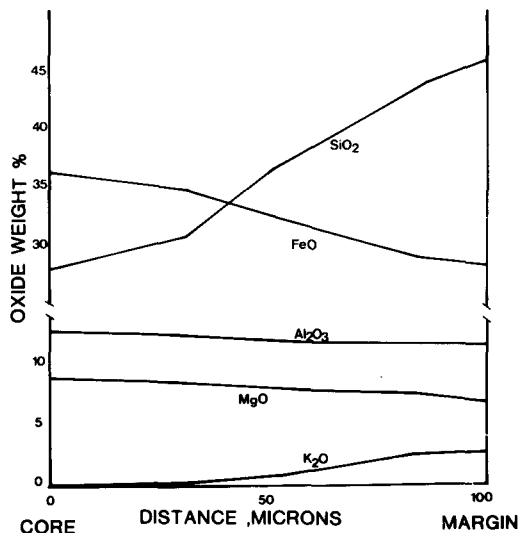


FIG. 3. Compositional variation diagram, illustrating the differences across a chlorite pseudomorph adjacent to quartz.

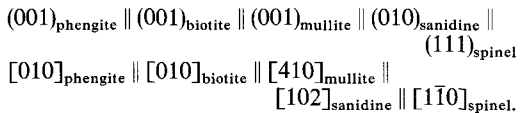
thickness. Statistical counting errors and errors involved in the calibration of standard materials results in an accuracy of about  $\pm 5\%$  for each oxide weight %.

### Examination of phengite pseudomorphs

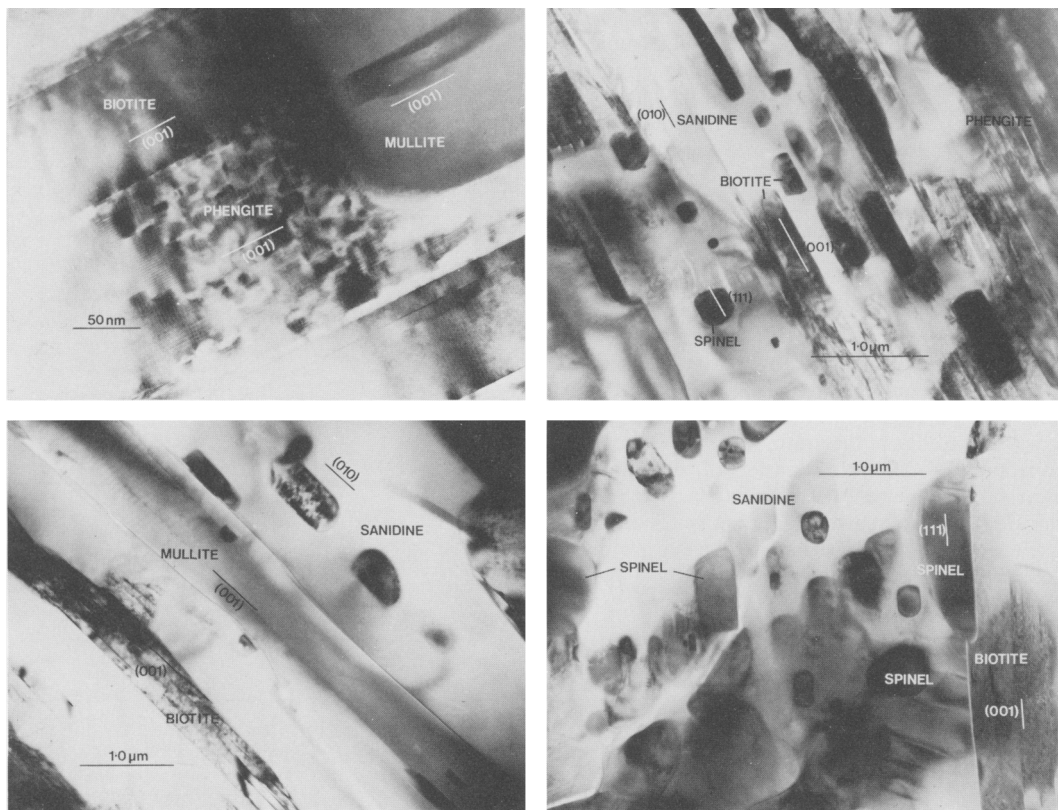
Upon examination of many thin foils the mineral assemblage of the partially reacted phengite grains has been found to consist of:

phengite + biotite + mullite + spinel + sanidine.

Figs. 4 to 7 illustrate this assemblage and demonstrate that there is a parallel elongation of all the phases. Fig. 4, a one-dimensional lattice image, shows that the (001) lattice planes of the phengite and biotite are parallel. On inspection of the diffraction patterns there is a consistent orientation relationship between the lattices of all five phases:



Also, the predominant interfaces of the phases tend to be parallel to (001) phengite as illustrated in Figs. 4 to 7. This is a reflection of surface energy, as will be discussed later. Figs. 4 to 6 are images from the centre of a pseudomorph grain showing moderate birefringence. From the microprobe data shown in Fig. 2 the aggregate compositions at these sites should be similar to that of unaltered phengite.



FIGS. 4-7. FIG. 4 (*top left*). A one-dimensional (001) lattice image of a partially reacted phengite grain. Orientation relationships between phengite and reaction products are illustrated. FIG. 5 (*top right*). Micrograph of a partially reacted phengite pseudomorph showing spinel and biotite in sanidine matrix with remnant phengite. FIG. 6 (*lower left*). Oriented, elongate grains of mullite and biotite in a sanidine matrix within a phengite pseudomorph. FIG. 7 (*lower right*). Assemblage of biotite, spinel and sanidine; micrograph recorded from near the edge of the phengite pseudomorph. Orientation relationships are only locally developed and there is no remnant phengite.

Fig. 7 is from near the edge of a pseudomorph. The microprobe data indicate that this site has undergone a greater metasomatic exchange of material than the areas shown in Figs. 4-6.

#### Analytical electron microscopy of phengite pseudomorphs

**Phengite.** Analyses of phengite are given in Table 3 and are similar to the microprobe analysis of unaltered Dalradian phengites given in Table 1. Many alkali-bearing minerals suffer alkali-element loss during analytical electron microscopy. This may be partially dealt with using the technique of McGill and Hubbard (1981), whereby analyses are performed for a range of live times and the measured alkali compositions are projected back to zero seconds on a plot of live time against oxide

weight %. The projected alkali content at zero seconds is usually close to a value appropriate for a stoichiometric formula. This procedure has been used in the cases of all alkali-bearing phases.

**Biotite.** Analyses of biotite are given in Table 4. In comparison to the biotite produced during regional metamorphism, these are richer in  $\text{Al}_2\text{O}_3$  and MgO as shown in Fig. 1. The high  $\text{Al}_2\text{O}_3$  weight % reflects the relatively Al-rich phengite precursor and the high Mg:Fe ratio may reflect the Mg-Fe partition coefficient between biotite and spinel, the biotite always having a lower Fe:Mg ratio than the spinel (see also Brearley, 1986).

**Mullite.** As shown in Table 5, mullite has a narrow compositional range. Weight percentages have been converted into a number of ions on the basis of 13 oxygens. All the iron is assumed to be present as  $\text{Fe}^{3+}$  substituting for Al.

# BREAKDOWN OF PHENGITE AND CHLORITE

111

Table 1 Microprobe analyses of regional metamorphic phengites

|                                |       |       |       |
|--------------------------------|-------|-------|-------|
| SiO <sub>2</sub>               | 46.55 | 45.76 | 48.57 |
| TiO <sub>2</sub>               | 0.55  | 0.51  | 0.57  |
| Al <sub>2</sub> O <sub>3</sub> | 29.21 | 28.71 | 27.14 |
| FeO                            | 2.92  | 3.02  | 4.23  |
| MnO                            | 0.00  | 0.00  | 0.00  |
| MgO                            | 1.04  | 1.49  | 1.79  |
| CaO                            | 0.00  | 0.00  | 0.00  |
| Na <sub>2</sub> O              | 0.42  | 0.44  | 0.00  |
| K <sub>2</sub> O               | 9.99  | 9.64  | 10.37 |
| Total                          | 91.38 | 89.57 | 92.67 |
| Si                             | 6.50  | 6.52  | 6.73  |
| Ti                             | 0.05  | 0.05  | 0.06  |
| Al                             | 4.92  | 4.82  | 4.43  |
| Fe                             | 0.34  | 0.36  | 0.49  |
| Mn                             | 0.00  | 0.00  | 0.00  |
| Mg                             | 0.22  | 0.32  | 0.37  |
| Ca                             | 0.00  | 0.00  | 0.00  |
| Na                             | 0.13  | 0.12  | 0.00  |
| K                              | 1.78  | 1.74  | 1.83  |
| O                              | 22.00 | 22.00 | 22.00 |

Table 2 Microprobe analyses of regional metamorphic chlorites

|                                |       |       |       |
|--------------------------------|-------|-------|-------|
| SiO <sub>2</sub>               | 23.41 | 24.14 | 24.88 |
| TiO <sub>2</sub>               | 0.00  | 0.00  | 0.00  |
| Al <sub>2</sub> O <sub>3</sub> | 20.93 | 21.33 | 21.01 |
| FeO                            | 33.18 | 32.75 | 30.66 |
| MnO                            | 0.00  | 0.00  | 0.00  |
| MgO                            | 8.39  | 9.56  | 11.28 |
| CaO                            | 0.00  | 0.00  | 0.00  |
| Na <sub>2</sub> O              | 0.00  | 0.00  | 0.00  |
| K <sub>2</sub> O               | 0.00  | 0.00  | 0.00  |
| Total                          | 85.91 | 87.68 | 88.15 |
| Si                             | 5.19  | 5.28  | 5.37  |
| Ti                             | 0.00  | 0.00  | 0.00  |
| Al                             | 5.47  | 5.48  | 5.35  |
| Fe                             | 6.15  | 6.00  | 5.54  |
| Mn                             | 0.00  | 0.00  | 0.00  |
| Mg                             | 2.77  | 3.12  | 3.63  |
| CaO                            | 0.00  | 0.00  | 0.00  |
| Na                             | 0.00  | 0.00  | 0.00  |
| K                              | 0.00  | 0.00  | 0.00  |
| O                              | 28.00 | 28.00 | 28.00 |

Table 3 Analyses of phengite from phengite pseudomorphs

|                                |        |        |        |
|--------------------------------|--------|--------|--------|
| SiO <sub>2</sub>               | 53.08  | 51.43  | 51.62  |
| TiO <sub>2</sub>               | 0.10   | 0.56   | 0.00   |
| Al <sub>2</sub> O <sub>3</sub> | 33.75  | 32.08  | 31.96  |
| FeO                            | 1.98   | 3.19   | 3.68   |
| MnO                            | 0.00   | 0.00   | 0.00   |
| MgO                            | 1.16   | 1.62   | 1.52   |
| CaO                            | 0.00   | 0.00   | 0.00   |
| Na <sub>2</sub> O              | 0.51   | 0.36   | 0.78   |
| K <sub>2</sub> O               | 9.42   | 10.76  | 10.43  |
| Total                          | 100.00 | 100.00 | 100.00 |
| Si                             | 6.59   | 6.55   | 6.58   |
| Ti                             | 0.01   | 0.05   | 0.00   |
| Al                             | 4.94   | 4.82   | 4.80   |
| Fe                             | 0.21   | 0.34   | 0.39   |
| Mn                             | 0.00   | 0.00   | 0.00   |
| Mg                             | 0.21   | 0.21   | 0.29   |
| Ca                             | 0.00   | 0.00   | 0.00   |
| Na                             | 0.06   | 0.10   | 0.19   |
| K                              | 1.50   | 1.75   | 1.70   |
| O                              | 22.00  | 22.00  | 22.00  |

Table 4 Analyses of biotite from phengite pseudomorphs

|                                |        |        |        |
|--------------------------------|--------|--------|--------|
| SiO <sub>2</sub>               | 38.13  | 40.05  | 41.21  |
| TiO <sub>2</sub>               | 1.58   | 0.00   | 2.01   |
| Al <sub>2</sub> O <sub>3</sub> | 23.20  | 22.62  | 21.16  |
| FeO                            | 13.75  | 12.98  | 13.17  |
| MnO                            | 0.00   | 0.00   | 0.00   |
| MgO                            | 13.58  | 15.61  | 14.84  |
| CaO                            | 0.00   | 0.00   | 0.00   |
| Na <sub>2</sub> O              | 0.62   | 0.37   | 0.40   |
| K <sub>2</sub> O               | 9.14   | 8.71   | 7.21   |
| Total                          | 100.00 | 100.00 | 100.00 |
| Si                             | 5.31   | 5.52   | 5.63   |
| Ti                             | 0.16   | 0.00   | 0.21   |
| Al                             | 3.81   | 3.68   | 3.41   |
| Fe                             | 1.60   | 1.51   | 1.50   |
| Mn                             | 0.00   | 0.00   | 0.00   |
| Mg                             | 2.83   | 3.21   | 3.02   |
| Ca                             | 0.00   | 0.00   | 0.00   |
| Na                             | 0.16   | 0.08   | 0.09   |
| K                              | 1.62   | 1.52   | 1.32   |
| O                              | 22.00  | 22.00  | 22.00  |

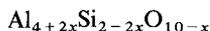
Table 5 Analyses of mullite from phengite pseudomorphs

|                                |        |        |        |
|--------------------------------|--------|--------|--------|
| SiO <sub>2</sub>               | 31.10  | 30.20  | 30.66  |
| TiO <sub>2</sub>               | 0.00   | 0.00   | 0.00   |
| Al <sub>2</sub> O <sub>3</sub> | 67.30  | 67.85  | 67.65  |
| FeO                            | 0.00   | 0.00   | 0.00   |
| Fe <sub>2</sub> O <sub>3</sub> | 1.09   | 1.04   | 1.42   |
| MnO                            | 0.00   | 0.00   | 0.00   |
| MgO                            | 0.60   | 0.91   | 0.27   |
| CaO                            | 0.00   | 0.00   | 0.00   |
| Na <sub>2</sub> O              | 0.00   | 0.00   | 0.00   |
| K <sub>2</sub> O               | 0.00   | 0.00   | 0.00   |
| Total                          | 100.00 | 100.00 | 100.00 |
| Si                             | 2.23   | 2.16   | 2.19   |
| Ti                             | 0.00   | 0.00   | 0.00   |
| Al                             | 5.56   | 5.61   | 5.58   |
| Fe <sup>2+</sup>               | 0.00   | 0.00   | 0.00   |
| Fe <sup>3+</sup>               | 0.06   | 0.06   | 0.08   |
| Mn                             | 0.00   | 0.00   | 0.00   |
| Mg                             | 0.06   | 0.09   | 0.03   |
| Ca                             | 0.00   | 0.00   | 0.00   |
| Na                             | 0.00   | 0.00   | 0.00   |
| K                              | 0.00   | 0.00   | 0.00   |
| O                              | 13.00  | 13.00  | 13.00  |

Table 6 Analyses of spinel from phengite pseudomorphs.

|                                |        |        |        |
|--------------------------------|--------|--------|--------|
| Al <sub>2</sub> O <sub>3</sub> | 60.61  | 57.38  | 59.69  |
| FeO                            | 28.23  | 27.94  | 29.36  |
| Fe <sub>2</sub> O <sub>3</sub> | 2.39   | 6.13   | 3.05   |
| MnO                            | 0.12   | 0.00   | 0.00   |
| MgO                            | 8.65   | 8.55   | 7.90   |
| Total                          | 100.00 | 100.00 | 100.00 |
| Al                             | 1.95   | 1.87   | 1.94   |
| Fe <sup>2+</sup>               | 0.65   | 0.63   | 0.68   |
| Fe <sup>3+</sup>               | 0.05   | 0.13   | 0.06   |
| Mn                             | 0.01   | 0.00   | 0.00   |
| Mg                             | 0.34   | 0.35   | 0.32   |
| O                              | 4.00   | 4.00   | 4.00   |

Much work has been performed on the alumina-rich part of the  $\text{Al}_2\text{O}_3$ - $\text{SiO}_2$  system, although mainly at liquidus temperatures. There is a degree of solid solution between sillimanite and mullite. Cameron (1977) envisaged diminishing solid solution between the two phases with decreasing temperature. Hariya *et al.* (1969) proposed that both pressure and temperature are important factors in determining solid solution and that the more dense sillimanite becomes predominant at high pressures. For the mullite analysed here, the value of  $x$  in the general mullite formula:



is 0.15. For stoichiometric  $3\text{Al}_2\text{O}_3 \cdot 2\text{SiO}_2$  mullite,  $x = 0.25$  and for sillimanite  $x = 0.00$ . The analysed mullites are intermediate between these two compositions and are indicative of a meta-stable mullite typical of very low pressures and moderate temperatures of 600–700 °C (Schreyer, 1976).

**Spinel.** Compositions of the spinels are given in Table 6 and are plotted on the ternary spinel-hercynite-magnetite diagram in Fig. 8. The small amount of magnetite component is probably related to the presence of ferric iron in the parent phengite rather than being due to later oxidation. The high  $\text{Fe}/(\text{Fe} + \text{Mg})$  ratio reflects the Fe-Mg partitioning behaviour between coexisting spinel and biotite; the spinel is always significantly richer in iron.

**Sanidine.** Feldspar analyses are given in Table 7. The sanidine, like the micas, suffers considerable alkali loss during normal live time analysis of 100 seconds. The McGill and Hubbard technique was employed as described for phengite to estimate true alkali oxide weight percentages. The  $\text{Na}/(\text{Na} + \text{K})$  ratio is about 0.3; this is very different from the

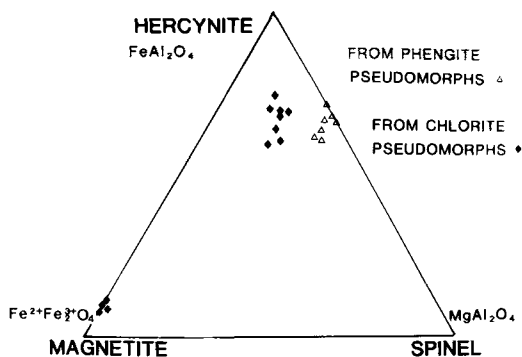


FIG. 8. Ternary spinel diagram, illustrating the compositional differences between spinel formed in phengite pseudomorphs and spinel formed in chlorite pseudomorphs.

compositions of the feldspar in the unaltered Dalradian rocks which are almost pure albite. The data of Martin (1972) concerning the alkali feldspar solvus at low pressures indicates minimum temperatures of 700 °C, assuming equilibrium conditions prevailed.

#### Examination of chlorite pseudomorphs

Pseudomorphs after regional chlorite consist of three types of mineral intergrowth, with assemblages depending upon the distance from the edge of the original chlorite grain. These are:

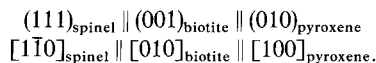
- A. chlorite, orthopyroxene, spinel (at centres of larger pseudomorphs);
- B. cordierite, spinel, magnetite, orthopyroxene (near edges of pseudomorphs);
- C. cordierite, spinel, orthopyroxene, biotite (near edges of pseudomorphs).

The relative orientation of phases is not as regular as that observed in the phengite pseudomorphs. For instance, in Fig. 9 chlorite shows curving (001) planes. This is typical of regional metamorphic chlorites, and is probably the result of deformation during the regional metamorphism.

Of all the reaction products cordierite tends to have formed the coarsest grains which measure 2–3  $\mu\text{m}$  in the longest dimension. The cordierite is locally altered to a highly disordered material that is easily damaged by the electron beam and hence likely to have a high water content (Hobbs, 1983). This material is probably the retrogressive breakdown product of cordierite known as 'pinitite', and further investigation of this material is in progress. In Fig. 12 it is clear that the pinitite has grown into the cordierite along the (010) plane. These planes are parallel to the tunnel structure in cordierite.

Orthopyroxene, in Fig. 9, has a modulated structure, indicative of disorder. The diffraction pattern shows a slight asterism also indicative of disorder.

No orientation relationships were observed between the small amount of remnant chlorite and its breakdown products. However the following relationships were observed between the breakdown products themselves:



#### Analytical electron microscopy of chlorite pseudomorphs

**Chlorite.** Analyses of remnant chlorite, given in Table 8, show a similar compositional range to chlorites in the regional metamorphic rocks from outside the thermal aureole.

Table 7 Analyses of alkali feldspar from phengite pseudomorphs

|                                |        |        |        |
|--------------------------------|--------|--------|--------|
| SiO <sub>2</sub>               | 66.22  | 66.98  | 66.17  |
| TiO <sub>2</sub>               | 0.41   | 0.24   | 0.17   |
| Al <sub>2</sub> O <sub>3</sub> | 20.03  | 20.12  | 19.61  |
| FeO                            | 0.71   | 0.75   | 0.48   |
| Fe <sub>2</sub> O <sub>3</sub> | 0.00   | 0.00   | 0.00   |
| MnO                            | 0.00   | 0.00   | 0.00   |
| MgO                            | 0.00   | 0.00   | 0.00   |
| CaO                            | 0.00   | 0.00   | 0.00   |
| Na <sub>2</sub> O              | 2.17   | 2.14   | 2.03   |
| K <sub>2</sub> O               | 10.47  | 9.77   | 11.54  |
| Total                          | 100.00 | 100.00 | 100.00 |
| Si                             | 2.99   | 2.99   | 2.97   |
| Ti                             | 0.01   | 0.01   | 0.01   |
| Al                             | 1.07   | 1.06   | 1.05   |
| Fe <sup>2+</sup>               | 0.02   | 0.03   | 0.01   |
| Fe <sup>3+</sup>               | 0.00   | 0.00   | 0.00   |
| Mn                             | 0.00   | 0.00   | 0.00   |
| Mg                             | 0.00   | 0.00   | 0.00   |
| Ca                             | 0.00   | 0.00   | 0.00   |
| Na                             | 0.19   | 0.19   | 0.18   |
| K                              | 0.61   | 0.56   | 0.67   |
| O                              | 8.00   | 8.00   | 8.00   |

Table 8 Analyses of chlorite from chlorite pseudomorphs

|                                |        |        |        |
|--------------------------------|--------|--------|--------|
| SiO <sub>2</sub>               | 27.58  | 27.24  | 27.55  |
| TiO <sub>2</sub>               | 0.00   | 0.00   | 0.00   |
| Al <sub>2</sub> O <sub>3</sub> | 24.34  | 24.36  | 24.35  |
| FeO                            | 36.84  | 38.62  | 37.20  |
| MnO                            | 0.00   | 0.00   | 0.00   |
| MgO                            | 11.24  | 9.78   | 10.90  |
| CaO                            | 0.00   | 0.00   | 0.00   |
| Na <sub>2</sub> O              | 0.00   | 0.00   | 0.00   |
| K <sub>2</sub> O               | 0.00   | 0.00   | 0.00   |
| Total                          | 100.00 | 100.00 | 100.00 |
| Si                             | 5.30   | 5.28   | 5.30   |
| Ti                             | 0.00   | 0.00   | 0.00   |
| Al                             | 5.30   | 5.56   | 5.52   |
| Fe                             | 5.91   | 6.25   | 5.97   |
| Mn                             | 0.00   | 0.00   | 0.00   |
| Mg                             | 3.21   | 2.82   | 3.11   |
| Ca                             | 0.00   | 0.00   | 0.00   |
| Na                             | 0.00   | 0.00   | 0.00   |
| K                              | 0.00   | 0.00   | 0.00   |
| O                              | 28.00  | 28.00  | 28.00  |

Table 9. Analyses of spinel and magnetite from chlorite pseudomorphs

|                                |        |        |        |        |
|--------------------------------|--------|--------|--------|--------|
| TiO <sub>2</sub>               | 0.62   | 0.72   | 0.00   | 0.00   |
| Al <sub>2</sub> O <sub>3</sub> | 54.45  | 52.24  | 54.68  | 5.93   |
| FeO                            | 33.79  | 34.17  | 36.05  | 32.06  |
| Fe <sub>2</sub> O <sub>3</sub> | 6.35   | 8.52   | 6.30   | 62.01  |
| MgO                            | 4.79   | 4.35   | 2.97   | 0.00   |
| Total                          | 100.00 | 100.00 | 100.00 | 100.00 |
| Ti                             | 0.01   | 0.02   | 0.00   | 0.00   |
| Al                             | 1.84   | 1.78   | 1.86   | 0.26   |
| Fe <sup>2+</sup>               | 0.81   | 0.83   | 0.87   | 1.00   |
| Fe <sup>3+</sup>               | 0.14   | 0.18   | 0.14   | 1.74   |
| Mg                             | 0.20   | 0.19   | 0.13   | 0.00   |

Table 10 Analyses of orthopyroxene from chlorite pseudomorphs

|                                |        |        |        |
|--------------------------------|--------|--------|--------|
| SiO <sub>2</sub>               | 48.01  | 43.39  | 49.56  |
| TiO <sub>2</sub>               | 0.00   | 0.00   | 0.00   |
| Al <sub>2</sub> O <sub>3</sub> | 4.88   | 7.79   | 6.07   |
| FeO                            | 29.91  | 32.03  | 29.15  |
| Fe <sub>2</sub> O <sub>3</sub> | 0.00   | 0.00   | 0.00   |
| MnO                            | 1.89   | 0.39   | 0.09   |
| MgO                            | 15.31  | 16.40  | 15.13  |
| CaO                            | 0.00   | 0.00   | 0.00   |
| Na <sub>2</sub> O              | 0.00   | 0.00   | 0.00   |
| K <sub>2</sub> O               | 0.00   | 0.00   | 0.00   |
| Total                          | 100.00 | 100.00 | 100.00 |
| Si                             | 1.87   | 1.71   | 1.89   |
| Ti                             | 0.00   | 0.00   | 0.00   |
| Al                             | 0.22   | 0.36   | 0.27   |
| Fe <sup>2+</sup>               | 0.97   | 1.06   | 0.90   |
| Fe <sup>3+</sup>               | 0.00   | 0.00   | 0.00   |
| Mn                             | 0.06   | 0.01   | 0.00   |
| Mg                             | 0.89   | 0.96   | 0.86   |
| Ca                             | 0.00   | 0.00   | 0.00   |
| Na                             | 0.00   | 0.00   | 0.00   |
| K                              | 0.00   | 0.00   | 0.00   |
| O                              | 6.00   | 6.00   | 6.00   |

Table 11 Analyses of cordierite from chlorite pseudomorphs

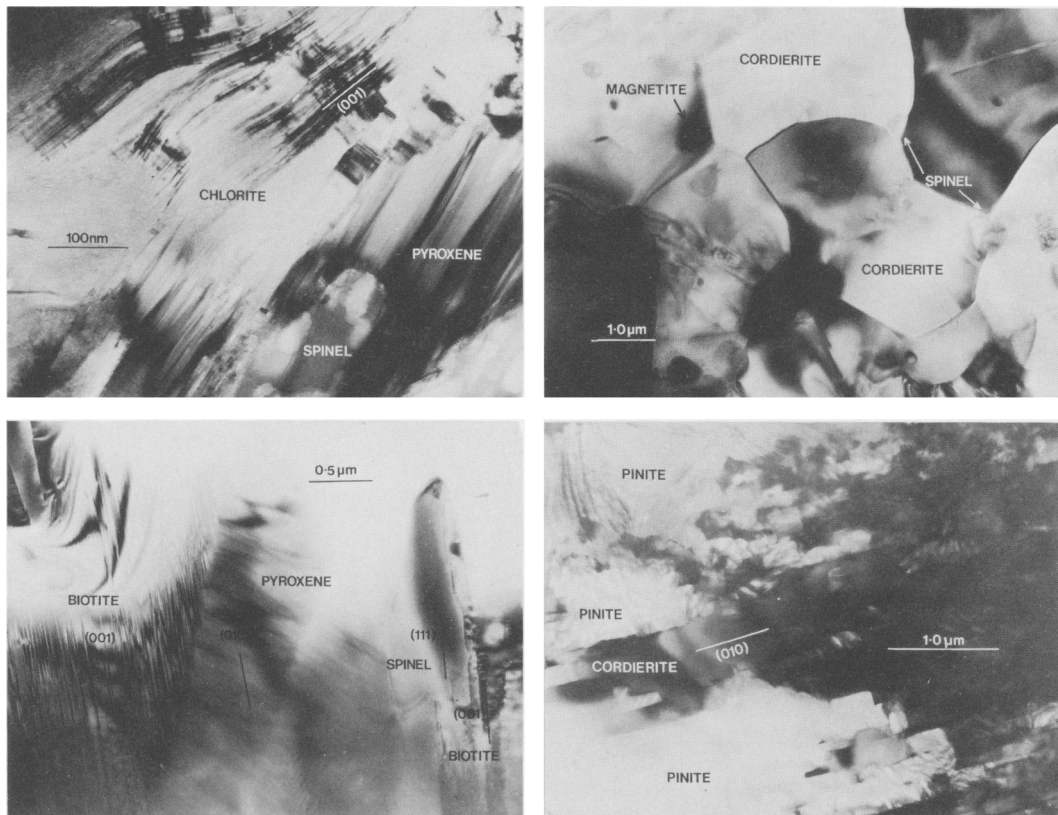
|                                |        |        |        |
|--------------------------------|--------|--------|--------|
| SiO <sub>2</sub>               | 50.29  | 48.33  | 49.95  |
| TiO <sub>2</sub>               | 0.00   | 0.00   | 0.00   |
| Al <sub>2</sub> O <sub>3</sub> | 33.09  | 33.78  | 33.16  |
| FeO                            | 10.47  | 11.27  | 9.55   |
| Fe <sub>2</sub> O <sub>3</sub> | 0.00   | 0.00   | 0.00   |
| MnO                            | 0.00   | 0.00   | 0.00   |
| MgO                            | 6.15   | 6.62   | 7.34   |
| CaO                            | 0.00   | 0.00   | 0.00   |
| Na <sub>2</sub> O              | 0.00   | 0.00   | 0.00   |
| K <sub>2</sub> O               | 0.00   | 0.00   | 0.00   |
| Total                          | 100.00 | 100.00 | 100.00 |
| Si                             | 5.11   | 4.95   | 5.06   |
| Ti                             | 0.00   | 0.00   | 0.00   |
| Al                             | 3.95   | 4.08   | 3.96   |
| Fe <sup>2+</sup>               | 0.88   | 0.96   | 0.81   |
| Fe <sup>3+</sup>               | 0.00   | 0.00   | 0.00   |
| Mn                             | 0.00   | 0.00   | 0.00   |
| Mg                             | 0.93   | 1.01   | 1.11   |
| Ca                             | 0.00   | 0.00   | 0.00   |
| Na                             | 0.00   | 0.00   | 0.00   |
| K                              | 0.00   | 0.00   | 0.00   |
| O                              | 18.00  | 18.00  | 18.00  |

Table 12 Analyses of biotite from chlorite pseudomorphs

|                                |        |        |        |
|--------------------------------|--------|--------|--------|
| SiO <sub>2</sub>               | 39.37  | 42.41  | 39.07  |
| TiO <sub>2</sub>               | 5.12   | 4.02   | 5.05   |
| Al <sub>2</sub> O <sub>3</sub> | 15.58  | 14.14  | 16.17  |
| FeO                            | 17.27  | 13.55  | 16.40  |
| MnO                            | 0.00   | 0.00   | 0.00   |
| MgO                            | 12.49  | 16.13  | 13.72  |
| CaO                            | 0.00   | 0.00   | 0.00   |
| Na <sub>2</sub> O              | 0.19   | 0.54   | 0.20   |
| K <sub>2</sub> O               | 9.98   | 9.20   | 9.39   |
| Total                          | 100.00 | 100.00 | 100.00 |
| Si                             | 5.64   | 5.92   | 5.56   |
| Ti                             | 0.55   | 0.41   | 0.54   |
| Al                             | 2.62   | 2.32   | 2.70   |
| Fe                             | 2.06   | 1.58   | 1.95   |
| Mn                             | 0.00   | 0.00   | 0.00   |
| Mg                             | 2.66   | 3.35   | 2.93   |
| Ca                             | 0.00   | 0.00   | 0.00   |
| Na                             | 0.04   | 0.07   | 0.03   |
| K                              | 1.83   | 1.64   | 1.70   |
| O                              | 22.00  | 22.00  | 22.00  |

*Spinel.* Analyses of spinels in chlorite pseudomorphs are given in Table 9; these spinels have larger concentrations of hercynite and magnetite components than spinels in the phengite pseudomorphs.

Magnetite is also present as a separate phase, and contains a small amount of hercynite component. The presence of magnetite and Fe<sup>3+</sup> in the hercynitic spinel may be partially due to the presence of ferric iron in the precursor chlorite, but may also



FIGS. 9-12. FIG. 9 (*top left*). Micrograph recorded from the centre of a large chlorite pseudomorph, showing remnant chlorite, with a deformed crystal lattice, and the reaction products spinel and pyroxene typical of intergrowth A. FIG. 10 (*top right*). Coarse-grained cordierite with small, rounded inclusions of spinel and magnetite, produced by a reaction between chlorite and quartz from near the edge of a chlorite pseudomorph. FIG. 11 (*lower left*). Oriented spinel, biotite and pyroxene produced by a reaction between chlorite and phengite from a pseudomorph of chlorite locally intergrown with phengite. FIG. 12 (*lower right*). Partially pinitised cordierite from within a chlorite pseudomorph. Pinitite has grown into cordierite along the (010) plane of cordierite.

be the result of oxidation. From a consideration of the compositions of these coexisting spinels and the experimental results of Turnock and Eugster (1962) for the hercynite-magnetite solvus, equilibrium temperatures are estimated to have been in the range 600–700 °C. There is no significant correlation of spinel compositions with local mineral assemblages.

**Orthopyroxene.** As the analyses in Table 10 show,  $\text{Al}_2\text{O}_3$  varies from 4 to 8 wt.%. Fujii (1976) demonstrated that in the orthopyroxene, spinel, forsterite system, the  $\text{Al}_2\text{O}_3$  content of orthopyroxene increases with increasing temperature at low pressures; an equilibrium composition of 8 wt. %  $\text{Al}_2\text{O}_3$  in orthopyroxene can only be achieved at temperatures in excess of 900 °C. This temperature is much higher than that estimated from other assemblages

in this study and probably indicates that the pyroxene did not achieve chemical equilibrium with the other reaction products. There is no consistent variation in either  $\text{Al}_2\text{O}_3$  or  $\text{Fe}/(\text{Fe} + \text{Mg})$  with the local assemblage, which provides further evidence of disequilibrium.

**Cordierite.** Analyses are given in Table 11. The  $\text{Fe}/(\text{Fe} + \text{Mg})$  ratio varies from about 0.4 to 0.5, not unusually high for cordierite in metapelites.

**Biotite.** Analyses are given in Table 12, and plotted in Fig. 1. These biotites are more magnesian than those of regional metamorphic origin and are significantly less aluminous than the biotites developed in phengite pseudomorphs. The high Mg content of biotites from the chlorite and phengite pseudomorphs reflects the strong partitioning of Fe into the coexisting spinel. The low Al content

probably reflects the relatively Al-poor parent chlorite.

### Discussion and interpretation of results

*Crystallography of reactions.* In the vast majority of solid-state reactions there is an orientation relationship between the participating phases, at least during nucleation and early growth. If there is some matching of crystal structures across inter-phase boundaries and the boundaries are coherent or semi-coherent the total surface energy involved in the reaction is minimised (Chadwick, 1971; Porter and Easterling, 1981). During later stages of growth or coarsening, coherency may be lost completely because the coherency strains become too large. The morphology of reacting phases is such that the coherent or semi-coherent (well-matched) interfaces are usually large and planar, whereas the incoherent interfaces are small and non-planar. An example of this can be seen in the phases that make up the phengite pseudomorph (Fig. 4–7) and in the intergrowths near the margins of chlorite pseudomorphs (intergrowth C shown in Fig. 11).

No definite orientation relationship has been found between the parent chlorite and its reaction products. The observation that the biotite/spinel relationship is the same in the chlorite and phengite pseudomorphs and that the biotite and chlorite structures are the most similar of all the phases involved in the reaction of chlorite, suggest that the initial reaction products nucleated and grew with a specific orientation relationship to the parent chlorite. However, as the regional metamorphic chlorite had been deformed, oriented nucleation at one site would not necessarily be oriented with respect to adjacent regions of chlorite crystal. Oriented new mineral growth from the breakdown of chlorite at one nucleation site, may be juxtaposed against adjacent regions of chlorite with which no specific orientation relationship exists. Where specific orientation relationships do exist in the chlorite pseudomorphs, the original chlorite grain may have been less deformed than shown in Fig. 9.

In intergrowth type B from chlorite pseudomorphs, cordierite, spinel and magnetite possess no specific orientation relationship. This may be the result of loss of coherency as the reaction proceeded. However, it is also possible that the observed random orientation of rounded spinel and magnetite particles (Fig. 10) within cordierite is the result of incoherent nucleation, a very unusual process, but one that has been suggested by Brearley and Champness (1986) for the exsolution of magnetite in garnet.

The numerous crystallographic orientation rela-

tionships observed in the phengite and chlorite pseudomorphs show that the reaction products have incorporated structural elements from the precursor minerals during the transformation reaction. For instance, it is significant that many of the lattice planes of the reaction products which have grown parallel to the (001) plane of the phengites (the plane of closest oxygen packing) are each the most close-packed planes in their respective crystals (i.e. (001) biotite, (010) sanidine and (111) spinel). This results in the minimisation of surface and strain energies and will require the least diffusion of cations. Spry (1969) discussed topotactic replacement mechanisms in terms of the concept of structural continuity. He stated that solid-state transformations generally proceed by a minimum rearrangement of material within a single crystal. Clearly this has been the case in the phengite pseudomorph.

### Chemistry of reactions

*Phengite sites.* In multi-component chemical systems, a simple graphical treatment of reactions is impossible unless a technique is employed to reduce the number of components by thermodynamically valid means. Such a method has been used for pelites by Thompson (1957) and made into a general method by Greenwood (1975). Phases of fixed composition that are common to the rocks being studied may be used as projection points onto a plane or volume in compositional space defined by the remaining components.

As Smith (1969) believed that each grain acted as an isolated chemical system during metamorphism,

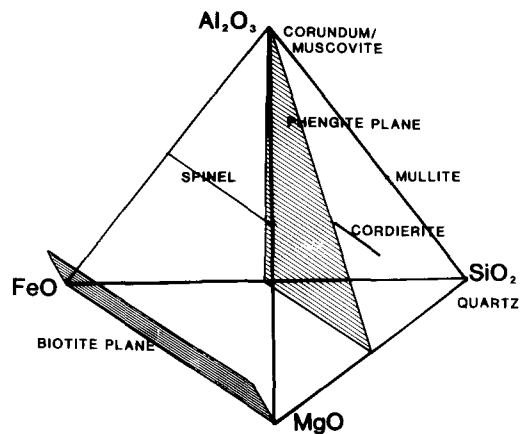
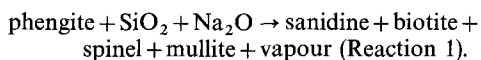


FIG. 13. FMAS diagram projected from K-feldspar and water, illustrating the phengite compositional range and compositions of phengite reaction products.

each phyllosilicate grain will be treated separately at first. The composition of phengite can be represented in the system  $K_2O$ - $MgO$ - $FeO$ - $Al_2O_3$ - $SiO_2$ - $H_2O$  (KFMASH). Water is assumed to be an excess component, leaving KMFAS. The initial projection is from K-feldspar into the system MFAS. This is shown in Fig. 13 with all reaction products and all possible phengite compositions plotted. Because individual compositions cannot be plotted uniquely on a drawing of a tetrahedron, a second projection from mullite is performed, eliminating  $SiO_2$  from the projected system. The phengite plane [A(FS)(MS)] is chosen as the plane of projection and is shown in Fig. 14 with the compositional ranges of all the relevant ferromagnesian phases; phengite, corundum and quartz (at infinity).

Fig. 14 shows the composition of precursor phengite and its reaction products. If the reaction was isochemical then corundum should also be present as one of the reaction products. The

absence of corundum suggests that there has been input of silica during the reaction, shifting the average composition of the phengite pseudomorphs onto the spinel-biotite join. On balancing the reaction (see Fig. 18) it is apparent that input of sodium is also necessary to account for the Na in the sanidine, over and above that provided by the phengite. The reaction may thus be written as:



It is interesting to compare this reaction with that proposed by other workers for similar reactions in natural environments. Smith (1969), using only theoretical considerations, proposed isochemical decomposition of phengite to produce sillimanite/mullite,  $\pm$  cordierite,  $\pm$  corundum  $\pm$  spinel + sanidine. He neglected the development of biotite, instead proposing cordierite, and ignored the possibility of migration of any components other than  $H_2O$ .

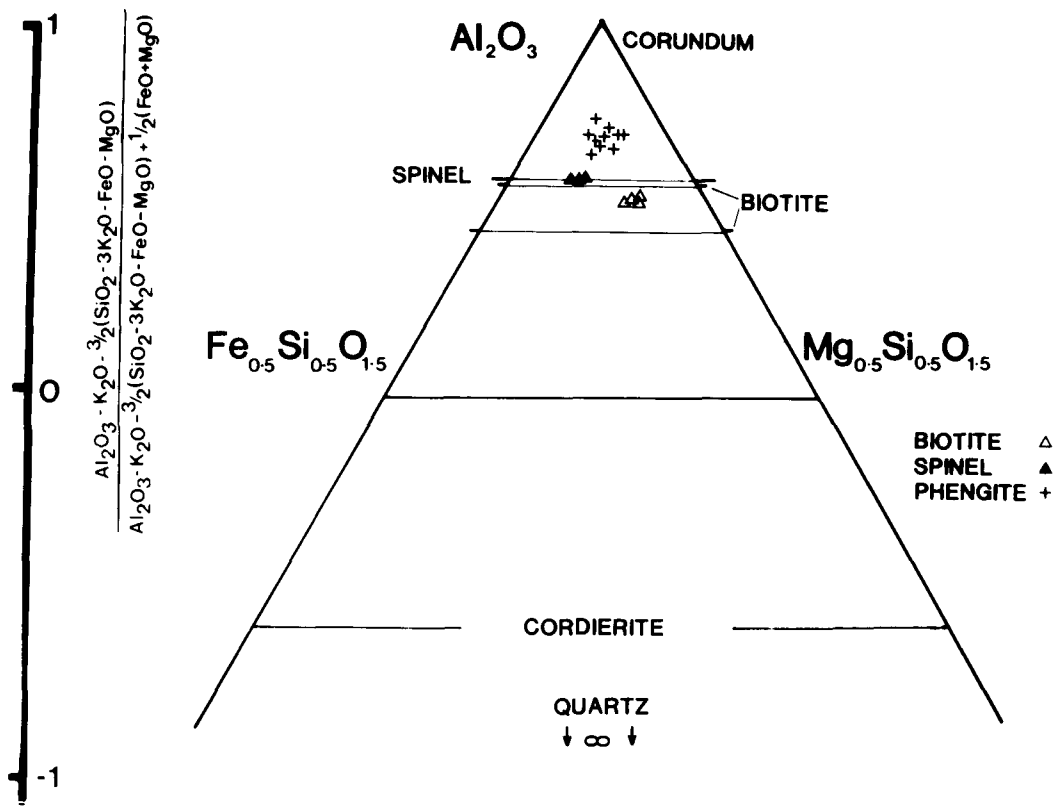
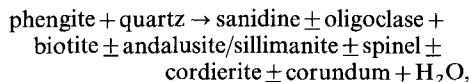


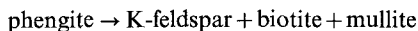
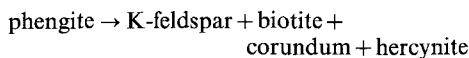
FIG. 14. A(FS)(MS) diagram projected from K-feldspar, mullite and water. Compositions of remnant phengite, and reaction products biotite and spinel are plotted. Note that phengite compositions lie away from the spinel biotite tie-line.

Wirth (1985) studied the contact metamorphism of phengite-bearing glaucophane schists and proposed the reaction



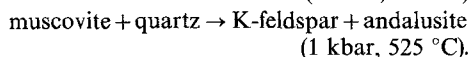
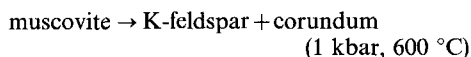
but he neglected to suggest specific assemblages. This reaction seems to imply a greater degree of interaction with the rest of the rock than in the reaction studied here. Also, assuming equilibrium conditions, it would appear unlikely that cordierite and corundum would be stable in the presence of  $\text{Al}_2\text{SiO}_5$  and sanidine, but metastable growth or growth in separate domains might enable such a mineral assemblage to exist in phengite pseudomorphs.

Brearley (1986) has suggested just such a domain development of mineral assemblages within phengite pseudomorphs. In a study of phengite breakdown in a small (< 1 m) pelitic xenolith from a dolerite sill, he proposed the reactions:



developing within a single crystal. The differences between these reactions and that proposed for this study are probably the result of different conditions of metamorphism. The time for reaction would have been much less, the temperatures of reaction would probably have been higher and there would have been less fluid available to aid melting and communication between reaction sites in Brearley's xenolith than in the outer zone of the aureole studied here.

It is also useful to examine the results of experiments performed on white micas under low-pressure, high-temperature conditions. Sundius and Bystrom (1953) studied phengite breakdown at 1000 °C and identified glass, mullite and an alumina phase. The time for reaction was very brief and temperatures much higher than those likely to have prevailed in our case. Thus it is not surprising that the reaction products are very different from those found in natural situations. Experiments performed on muscovite under equilibrium conditions by Yoder and Eugster (1955), Chatterjee and Johannes (1974) and Evans (1965) predict the reactions:



Such data must be considered carefully in relation to the phengite breakdown in this study because, although the low activity of the muscovite

component in the phengite may have the effect of depressing the equilibrium temperature of reaction at constant pressure and  $a_{\text{H}_2\text{O}}$  (as shown by Ferguson and Al Ameen, 1985), the natural situation under study may have suffered large overstepping of the equilibrium reaction curves. The experimental data predict that phengite should dehydrate at a temperature of about 600 °C. This is in approximate agreement with temperatures indicated by mineral solvi, implying that overstepping may not have been very great.

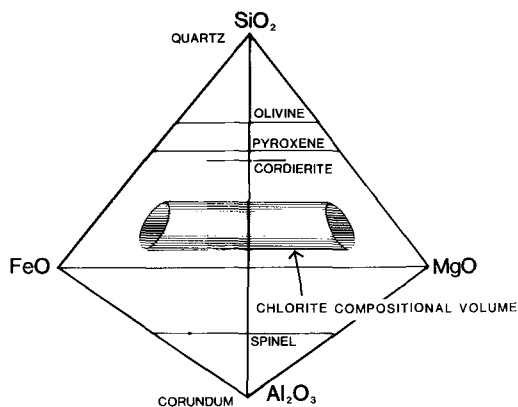
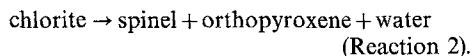


FIG. 15. FMAS diagram projected from water, illustrating the chlorite compositional range and compositions of possible breakdown products.

*Intergrowth A in the chlorite pseudomorphs.* Chlorite may be effectively described by the components  $\text{MgO-FeO-Al}_2\text{O}_3\text{-SiO}_2\text{-H}_2\text{O}$ . Water is assumed to be an excess component. The remaining quaternary system is shown in Fig. 15. Chlorite occupies a volume in compositional space because it can undergo Fe-Mg and Tschermak substitutions. All the phases found in intergrowth A are plotted in the compositional space. Spinel is chosen as the projection point as it is present in all the chlorite pseudomorph intergrowths and has a reasonably fixed composition. Projection is made from the average spinel composition  $\text{Hc}_{0.8}\text{Sp}_{0.2}$  on to the  $\text{FeO-MgO-SiO}_2$  plane (Fig. 16). Chlorite analyses fall on, or very near to, the pyroxene compositional range. Thus intergrowth A may be explained by the reaction:



The slight discrepancy in the chlorite composition in relation to the orthopyroxene may be explained by the presence of  $\text{Fe}^{3+}$  in the original

chlorite resulting in a magnetite component in the spinel (not accounted for in the projection). The  $\text{Fe}^{3+}$  content necessarily reduces the  $\text{Fe}^{2+}$  total and moves the projected average chlorite composition directly over the projected pyroxene compositions.

*Intergrowth B in the chlorite pseudomorphs.* The mineral assemblage found in this case may also be represented on Fig. 16, although magnetite must also be used as a projection point. It would appear that oxidation has occurred, increasing the  $\text{Fe}^{3+}$  total and reducing the  $\text{Fe}^{2+}$ . Also, as with the phengite, there has been an influx of silica. This causes the chlorite compositional range to lie between the pyroxene and cordierite compositional ranges. The local reaction responsible for intergrowth type B can therefore be written:

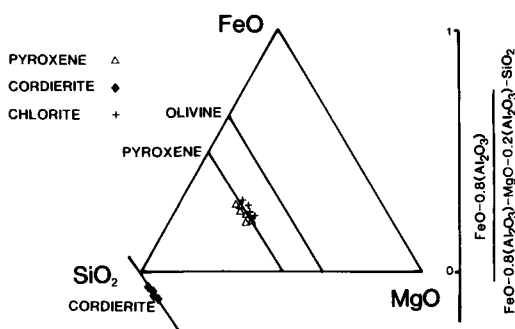
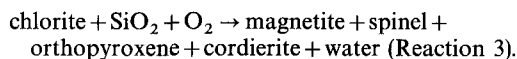
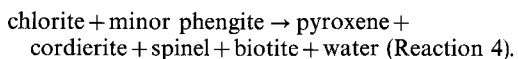


FIG. 16. SFM diagram projected from spinel ( $\text{Hc}_{0.8}\text{Sp}_{0.2}$ ) and water. Remnant chlorite compositions and the reaction products orthopyroxene and cordierite are plotted.

*Intergrowth C in the chlorite pseudomorphs.* The presence of the potassium-bearing biotite implies a significant degree of interaction between chlorite and a K-rich phase. The only K-bearing phase in the regional metamorphic rocks is phengite, which is locally coarsely intergrown with the chlorite.

In order to produce a phase diagram on which both phengite and chlorite can be plotted we must assume that  $\text{FeO}$  and  $\text{MgO}$  behave as a single component in the system  $\text{FeO}-\text{MgO}-\text{Al}_2\text{O}_3-\text{SiO}_2-\text{K}_2\text{O}-\text{H}_2\text{O}$ . Water is treated as an excess component, leaving  $(\text{Fe,Mg})\text{O}-\text{Al}_2\text{O}_3-\text{SiO}_2-\text{K}_2\text{O}$ . To reduce the system further, a projection is made from spinel, the most ubiquitous phase, onto the  $(\text{Fe,Mg})\text{O}-\text{SiO}_2-\text{K}_2\text{Si}_3\text{O}_7$  plane. The resulting phase diagram is shown in Fig. 17. The bulk composition of intergrowth C plots to the left-hand

side of the diagram in the cordierite-biotite-orthopyroxene field. A reaction between chlorite and phengite with the former well in excess of the latter could produce intergrowth C by the reaction:



A reaction between phengite and chlorite with the latter as the minor phase could still result in an assemblage identical to that produced by reaction 1 in the phengite pseudomorphs although, necessarily, the proportions of the reaction products would be different. A reaction between approximately equal proportions of chlorite and phengite may have produced the assemblage spinel + biotite + cordierite + K-feldspar.

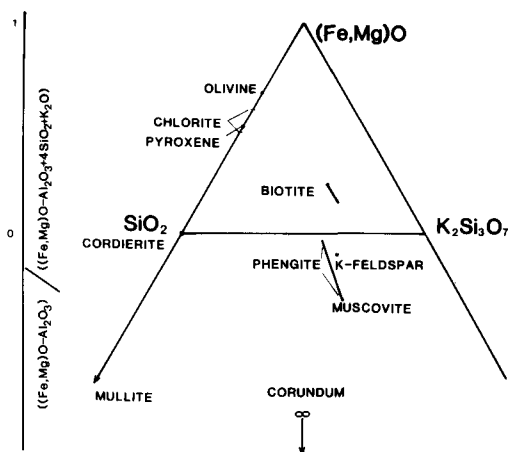


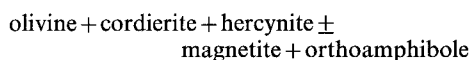
FIG. 17. S(FM)(SK) diagram projected from spinel and water. Compositions of phengite, chlorite and all their possible breakdown products are plotted.

Whether reaction 2, 3 or 4 took place would depend on the supply of necessary materials, and therefore upon which phases originally contacted the chlorite in the regional metamorphic precursor rock. In the case of reaction 2, the degree of isolation of the reaction site is also of great importance; only those areas of chlorite grains effectively isolated from the rest of the rock can have undergone breakdown by this reaction.

In order to ascertain whether or not the breakdown products of chlorite grew metastably, it is useful to compare the observed product assemblages with the results of experimental work on chlorite dehydration equilibria at low pressures and high temperatures.

Fawcett and Yoder (1966) worked on the Mg

end-member clinocllore at low pressure and showed that, in the absence of quartz, clorite breaks down at 1 kbar and 670 °C to produce forsterite, cordierite and spinel. In the presence of quartz, chlorite breaks down at 550 °C to produce talc and cordierite. James *et al.* (1975) studied the Fe end-member daphnite. Reaction products and temperatures depend on oxygen fugacity as well as pressure and temperature. For the QFM oxygen buffer, daphnite breaks down at 520 °C and 1 kbar to produce magnetite, cordierite and quartz. McOnie *et al.* (1975) studied the breakdown of chlorites of intermediate composition. For chlorites with Fe/Mg ratios similar to those of this study, the reaction products would be



at temperatures of about 650 °C.

Moreover, McOnie *et al.* (1975) also state that the assemblage enstatite+spinel is stable only above 3.25 kbar and 700 °C. The equilibrium involved in this case is:

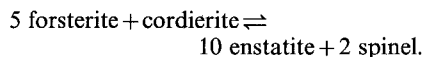


Fig. 2 of Fawcett and Yoder (1966) may be contoured for various values of  $\ln K$  for this equilibrium where  $K$  is the equilibrium constant and  $a$  is the activity:

$$\ln K = 10 \ln a_{\text{en}}^{\text{ppx}} + 2 \ln a_{\text{Mg-spinel}}^{\text{spinel}} - \ln a_{\text{Mg-cord}}^{\text{cord}} - 5 \ln a_{\text{fo}}^{\text{ol}}$$

For the mineral compositions observed in this study the equilibrium constant would be dominated by the activities of the orthopyroxene (because it has a coefficient of 10) and spinel (because it has such low Mg content). The mineral assemblage spinel + orthopyroxene is thus stable at much lower pressures in natural pelitic systems than in the pure MAS system.

Similarly the equilibrium position of the reaction: clinocllore = forsterite + enstatite + spinel + water would occur at lower temperatures in the natural, multicomponent assemblage than in the pure MAS system. Fawcett and Yoder (1966) have located the equilibrium curve for the Mg end-members at 700 °C at 1 kbar. However, as with phengite, significant overstepping of equilibrium reaction curves is likely to have occurred, and the probable temperatures of reaction would be close to 700 °C

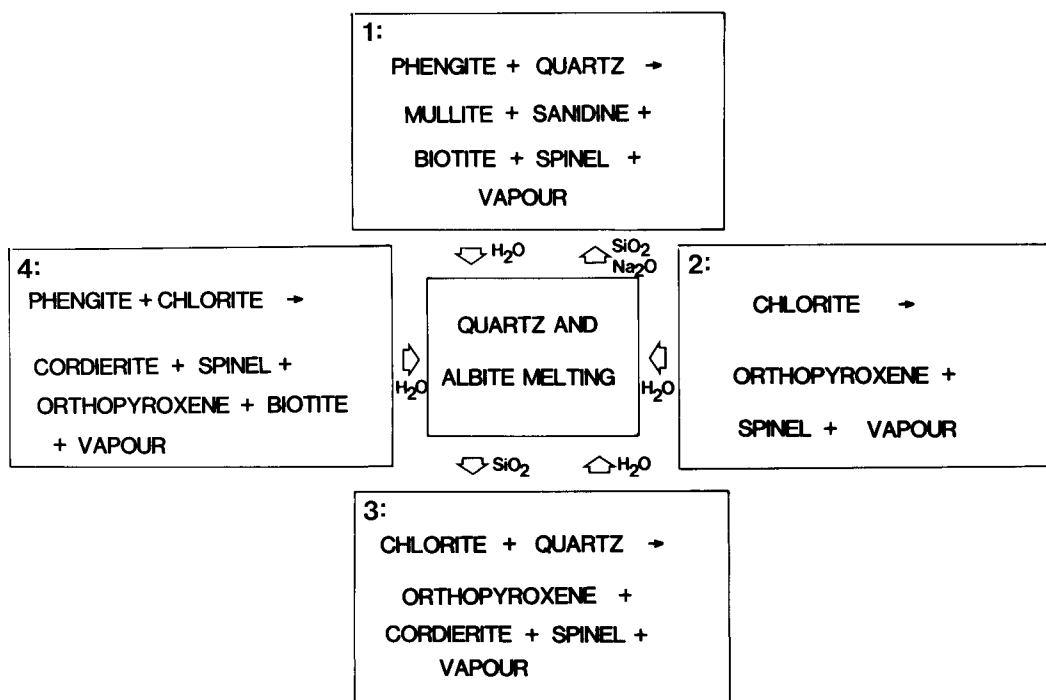


FIG. 18. A diagram relating the four phyllosilicate decomposition reactions to quartz and albite melting along grain boundaries. Fluid released during dehydration promotes the melting and facilitates diffusive interaction within the rock.

as indicated by mineral solvi. The presence of extra phases near the sites of reaction may increase the stability field of reaction products by reducing the temperatures of reaction. This might explain why the intergrowths that have suffered most interaction with the rest of the rock (i.e. chlorite pseudomorph intergrowths C and B) contain no relict, unreacted chlorite, whereas the isolated reaction sites have undergone only partial decomposition to chlorite.

*Chemical communication between reaction sites.* As discussed above, there is clear evidence for the influx of chemical components (particularly SiO<sub>2</sub>) to the phyllosilicate reaction sites. Thermal decomposition of phyllosilicates to assemblages of biotite and anhydrous minerals clearly involved dehydration. The vapour produced in this breakdown will have diffused into the surrounding mineral assemblages and will have promoted the melting of quartz and albite along grain boundaries. Once formed, the semi-continuous films of melt are likely to have provided routes for rapid diffusion, thus increasing the degree of interaction between grains.

This melt is the most likely source of the silica involved in reactions 1, 3 and 4. Likewise, the sodium involved in reaction 1 will have originated in the melt produced along albite grain boundaries.

Interactions between phyllosilicates, vapour and melt are shown schematically in Fig. 18, which is a summary of all the reactions discussed.

### Conclusions

Kinetically frozen phyllosilicate dehydration reactions have been observed in thermally metamorphosed semi-pelites from the outer aureole of the Sithean Sluagh intrusion. Reaction products are extremely fine-grained (< 2 μm) and cannot be resolved optically. Electron microscopy has revealed that phengite has broken down to spinel, mullite, sanidine and biotite and that chlorite has broken down to combinations of spinel, magnetite, biotite, orthopyroxene, cordierite and magnetite.

Specific crystallographic orientation relationships exist between product grains and relict phyllosilicates. In most cases the product grains are orientated with their closest-packed oxygen planes parallel to those of the precursor sheet-silicate. This minimises the surface and strain energies involved in the reaction and requires the least diffusion.

Despite the fact that the reactions did not go to completion and were short-lived, phengite and chlorite dehydration sites did not behave as closed systems.

### Acknowledgements

The authors would like to thank Graham Cliff, Ian Brough and Peter Kenway of the joint UMIST/Manchester University Metallurgy Department for technical assistance with the TEM work and Dr A. J. Brearley for valuable discussions and comments on the manuscript. The work was partly funded by the NERC research studentship GT4/84/GS/73. The Philips EM 400T was partly funded by the Natural Environment Research Council (Grant GR3/3580).

### References

- Barber, D. J. (1970) *J. Mater. Sci.* **5**, 1–8.  
 Brearley, A. J. (1984). Unpubl. Ph.D. thesis, University of Manchester.  
 — (1986) *Mineral. Mag.* **50**, 385–97.  
 — and Champness, P. E. (1986) *Ibid.* **50**, 621–33.  
 Cameron, W. E. (1977) *Am. Mineral.* **62**, 747–55.  
 Carmichael, D. M. (1969) *Contrib. Mineral. Petrol.* **20**, 244–67.  
 Chadwick, G. A. (1972) *Metallography of phase transformations*. Butterworths, London.  
 Chatterjee, N. D. and Johannes, W. (1974) *Contrib. Mineral. Petrol.* **48**, 89–114.  
 Chinner, G. A. (1962) *J. Petrol.* **2**, 312–23.  
 Cliff, G. and Lorimer, G. W. (1975) *J. Microsc.* **103**, 203–7.  
 Evans, B. W. (1965) *Am. J. Sci.* **263**, 647–67.  
 Fawcett, J. J. and Yoder, H. S. (1966) *Am. Mineral.* **51**, 353–80.  
 Ferguson, C. C. and Al-Ameen, S. I. (1985) *Mineral. Mag.* **49**, 505–14.  
 Foster, C. T. R. (1977) *Am. Mineral.* **62**, 727–46.  
 Fujii, T. (1976) *Carnegie Inst. Washington Ann. Report Div. Geophys. Lab.*, 1975–1976, 566–71.  
 Greenwood, H. J. (1975) *Am. Mineral.* **60**, 1–8.  
 Guidotti, C. V. (1973) *Contrib. Mineral. Petrol.* **42**, 33–42.  
 Hariya, Y., Dollase, W. A. and Kennedy, G. C. (1969) *Am. Mineral.* **54**, 1419–40.  
 Hey, M. M. (1954) *Mineral. Mag.* **30**, 277–92.  
 Hill, J. E. *et al.* (1905) *The geology of mid-Argyll*. Mem. Geol. Surv. Scotland.  
 Hobbs, L. (1983) Proc. 41st Ann. Meeting E.M.S.A., 346–349.  
 James, R. S., Turnock, A. C. and Fawcett, J. J. (1975) *Contrib. Mineral. Petrol.* **56**, 1–25.  
 Kwak, T. A. P. (1968) *Geochim. Cosmochim. Acta*, **32**, 1222–9.  
 Martin, R. F. (1972) In *The Feldspars* (MacKenzie, W. S. and Zussman, J., eds). Proceedings of a NATO Advanced Study Institute.  
 McGill, R. J., and Hubbard, F. H. (1981) In *Qualitative microanalysis with high spatial resolution* (Lorimer, G. W., Jacob, M. H. and Doig, P., eds.) The Metals Society.  
 McOnie, A. W., Fawcett, J. J. and James, R. S. (1975) *Am. Mineral.* **60**, 1047–62.  
 Miyashiro, A. (1973) *Metamorphism and metamorphic belts*. George Allen and Unwin.

- Porter, D. A. and Easterling, K. E. (1981) *Phase transformations in metals and alloys*. Van Nostrand Reinhold (U.K.) Co. Ltd.
- Schreyer, W. (1976) In *The evolution of the crystalline rocks* (Bailey, D. K. and Macdonald, R. eds), London and New York Academic Press.
- Smith, D. G. W. (1965) *Am. Mineral.* **50**, 1982–2022.
- (1969) *J. Petrol.* **10**, 20–55.
- Spry, A. (1969) *Metamorphic textures*, Pergamon Press.
- Sundius, N. and Bystrom, A. M. (1953) *Trans. Brit. Ceram. Soc.* **52**, 632–42.
- Thompson, J. B. (1957) *Am. Mineral.* **42**, 842–58.
- Tighe, N. J. (1976) In *Electron microscopy in mineralogy*. (Wenk, H. R., ed.). Berlin, Springer-Verlag.
- Turnock, A. C. and Eugster, H. P. (1962) *J. Petrol.* **3**, 533–65.
- Wirth, R. (1985) *Neues. Jahrb. Mineral. Abh.* **152**, 101–12.
- Yoder, H. S. and Eugster, H. P. (1955) *Geochim. Cosmochim. Acta* **6**, 225–80.

[Revised manuscript received 31 July 1986]